Design, simulation and analysis of a digital RF MEMS varactor using thick SU8 polymer

Microsyst Technol
DOI 10.1007/s00542-017-3371-3

TECHNICAL PAPER

Design, simulation and analysis of a digital RF MEMS varactor using thick SU-8 polymer

Noor Amalina Ramli[1] · Tughrul Arslan[1,2] · Nakul Haridas[2] · Wei Zhou[2]

Received: 1 September 2016 / Accepted: 15 March 2017

Abstract This paper presents the design, simulation and analysis of a 5-bit RF MEMS digital variable capacitor using thick SU-8 polymer to achieve both high capacitance ratio (C_r) and Q-factor. The proposed varactor design consists of five capacitive shunt switches loaded over a co-planar waveguide (CPW) line. This results 32 capacitance steps ranging from 102.23 fF to 3.57 pF ($C_r = 35$). The high capacitance ratio of the varactor is achieved by implementing SU-8 polymer as the base structure of the capacitor due to its low dielectric constant ($\varepsilon_r = 4$) hence reducing the overall minimum capacitance (C_{min}). The optimization of the SU-8 thickness has been carried out to get the optimum capacitance ratio and Q-factor. Moreover, the inclusion of semi-elliptical slot at the ground of CPW and variable sizes of CPW line further reduce the parasitic capacitance. To improve the reliability of the variable capacitor design, a new aluminium (Al) stopper design is used to prevent contact between the beams and the pull-down electrodes. Mechanical simulations and analysis have been carried out to investigate the effects of in-plane residual stress and stress gradient on the spring constant and the initial displacement of the proposed horizontal truss fixed–fixed beam structure. Compared to the conventional doubly clamped solid beam design, the proposed beam has less sensitivity to in-plane residual stress. This makes the pull in voltage to be less affected by the stress due to the fabrication. The simulated pull-in and lift-off voltages are 30 and 25 V respectively while the estimated switching time for the beam is 4.64 μs. The overall size of the varactor is 740 μm × 653 μm. The proposed RF MEMS varactor could be integrated in reconfigurable filters, phase shifters and matching networks targeting future multi-standard wireless communication systems.

1 Introduction

Due to rapid development in wireless communication in recent years, a lot of research have been carried out to realise multiband and reconfigurable front-end components to deal with ever increasing wireless communication standards. In order to support these standards such as GSM, WiFi, LTE, and Bluetooth, low power and compact size devices are required. In the RF transceiver part, tuning and reconfigurable elements such as tunable filters, matching networks and phase shifters play an important role to support these bands without increasing its overall size. Variable capacitors are one of the key components used in these systems. Commercially available solid-state varactors such as p-n junction diodes and Schottky diodes offer wide tuning range, small size and very fast tuning speed (Rebeiz 2003; Reinke 2011). However, they suffer from low power handling, low Q-factor, non-linearity effect, and high loss especially at high frequency bands. With the advent of the microelectromechanical systems (MEMS) technology, MEMS based varactors are seen as the best candidates to

✉ Noor Amalina Ramli
N.Ramli@ed.ac.uk

Tughrul Arslan
Tughrul.Arslan@ed.ac.uk

Nakul Haridas
N.Haridas@sofant.com

Wei Zhou
Wei.Zhou@sofant.com

[1] E-Wireless Research Group (E-Wireless), University of Edinburgh, Edinburgh EH9 3FF, UK

[2] Sofant Technologies, Scottish Microelectronics Centre, Edinburgh EH9 3FF, UK

Published online: 21 March 2017

replace the solid-state varactors. The main advantages of MEMS varactors over the conventional solid-state technology are low loss, zero power consumption (electrostatic actuation), high-Q factor and high linearity with respect to RF power (Gupta et al. 2013; Reinke 2011). In general, there are two types of MEMS varactors: analog and digital. Various analog and digital MEMS designs have been demonstrated in the literature (Gupta et al. 2013; McFeetors and Okoniewski 2007; Patel and Rebeiz 2012; Reinke 2011). One of the limitations that hampers the performance of analog designs is its low tuning ratio which is important to obtain wider tunability characteristic due to pull-in effect. This phenomena can be explained by the mechanical instability between electrostatic forces and restoring forces of the varactor structure, which causes the metal bridge to snap down when it reaches one-third of the air gap (Gupta et al. 2013; McFeetors and Okoniewski 2007). One way to achieve higher capacitance range is by employing digital type MEMS varactors or switched capacitor banks (Bakrikassem 2007; Dussopt and Rebeiz 2003). Digital MEMS varactors are formed by several switches loaded on a transmission line where the capacitance values are selected by switching ON and OFF the switches. The capacitance ratio of digital varactors can be calculated by finding the ratio of the maximum and minimum capacitance values obtained when all switches are in ON states and OFF states respectively. However, the capacitance ratio of the digital design is still limited by a high minimum capacitance (C_{min}) value originating from the fringing field and parasitic capacitance between the silicon substrate and coplanar waveguide.

SU-8 is a polymer that is widely used in MEMS devices especially for MEMS sensor as photo-resist sacrificial mask and to construct high aspect ratio structure (Melai et al. 2007) due to its thermal and chemical stability in the fabrication process. Recently, SU-8 was used as a passivation layer to elevate co-planar waveguide (CPW) for realising a low loss transmission line using low resistivity silicon wafer ($\rho < 100\ \Omega$ cm). (Lucibello et al. 2013; Marcelli et al. 2008) had used SU-8 as a lateral support for RF MEMS switch and sacrificial layer. Our previous work reported that by depositing and patterning 25 µm thick SU-8 layer on a silicon substrate, the parasitic capacitance due to fringing field and loss of the varactor could be reduced, hence increasing the capacitance ratio and the Q-factor of the proposed RF MEMS varactor (Ramli et al. 2016a, b). In this paper, an optimisation of the SU-8 layer thickness has been carried out to produce the optimal value of the capacitance ratio and the Q-factor. In addition, mechanical simulations have been conducted using the finite element method (FEM) software, CoventorWare™ to investigate the effects of in-plane residual stress and stress gradient on the spring constant and the initial displacement of the beam structure. A comparison between the proposed truss fixed–fixed beam design and conventional solid beam in terms of pull-in voltage and their tolerance towards in-plane stress and stress gradient is presented.

2 Design of the RF MEMS varactor

Digital MEMS varactors operate as a typical MEMS capacitive switch based on mechanical movement in lateral or vertical direction to achieve ON and OFF states (Rebeiz 2003). Normally, they are made of an array of shunt switches suspended over the centre conductor of a co-planar waveguide (CPW). Both ends of the switches are fixed to the ground to realize a digital varactor design. The bottom electrode under the beam provides the electrostatic actuation while RF capacitance is created between the suspended beam and the transmission line. The minimum capacitance is obtained when all the switches are in the upstate position; while the maximum value is achieved when all the beams are pulled down. The minimum capacitance during upstate condition, C_u can be calculated as

$$C_u = \frac{\varepsilon_0 A}{g_0 + \frac{t_d}{\varepsilon_r}} + C_f \tag{1}$$

where $\varepsilon_0 = 8.854 \times 10^{-12}$ is the permittivity of free space, A is the contact area of the both plates, g_0 is the initial gap, t_d is the dielectric thickness, and ε_r is relative dielectric constant. Typically, additional fringing field, C_f will contributes around 20–60% of the overall capacitance when the switch is on upstate position (Ramli et al. 2016a, b; Rebeiz 2003). The maximum capacitance of the varactor in the downstate position, C_d is given by

$$C_d = \frac{\varepsilon_0 \varepsilon_r A}{t_d} \tag{2}$$

The overall capacitance ratio of a digital varactor is defined as (Rebeiz 2003)

$$C_r = \frac{C_{d(\max)}}{C_{u(\min)}} \tag{3}$$

Figure 1 presents the top view of the proposed digital variable capacitor. The design consists of 5-bit binary weighted capacitive shunt switches over a co-planar waveguide (CPW) transmission line. The binary weighted capacitance values are calculated by varying the contact areas between the centre conductor of the CPW line and the bridges using (1) and (2).

The RF MEMS varactor is developed to achieve a high tuning range and Q-factor by utilising SU-8 technology. The parasitic capacitance is reduced by elevating the varactor from the silicon substrate by

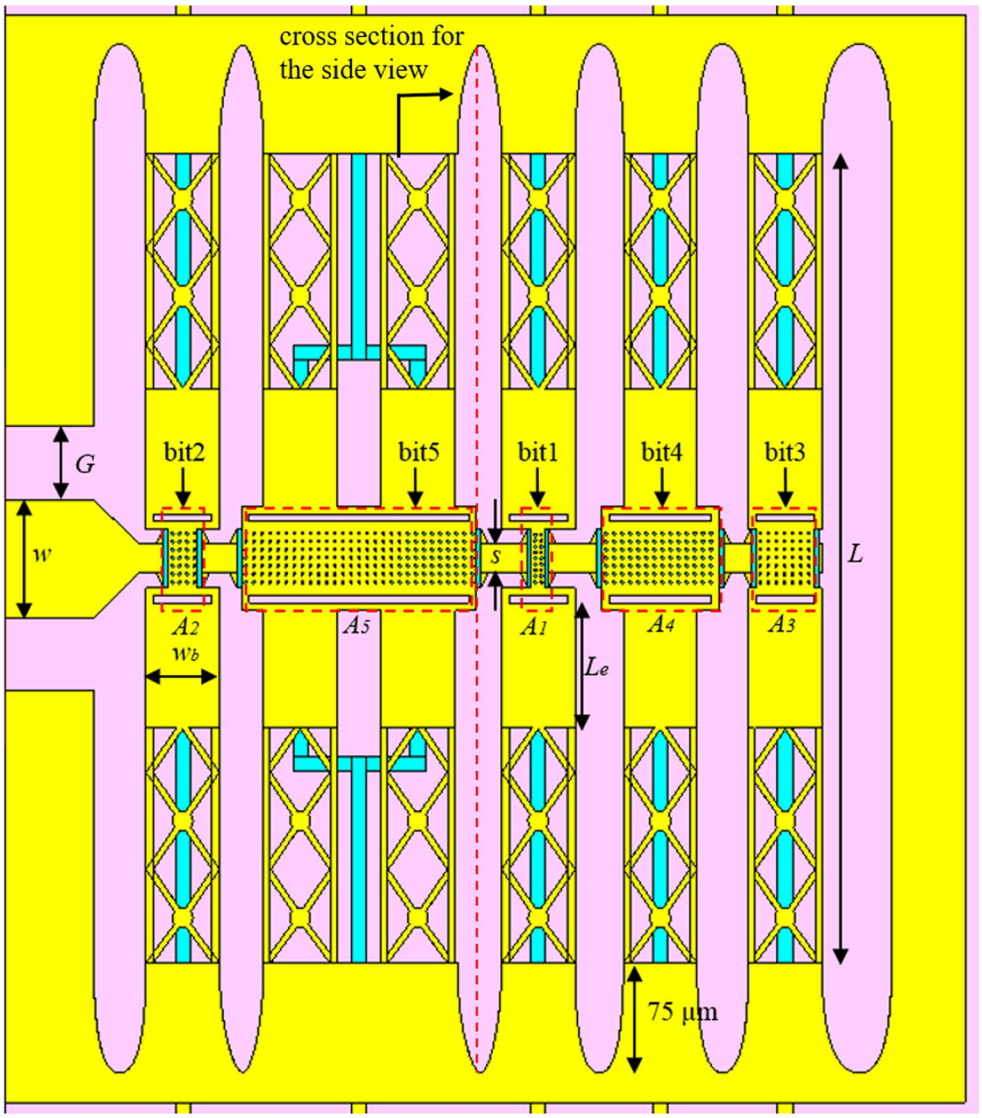

Fig. 1 5-bit RF MEMS digital varactor

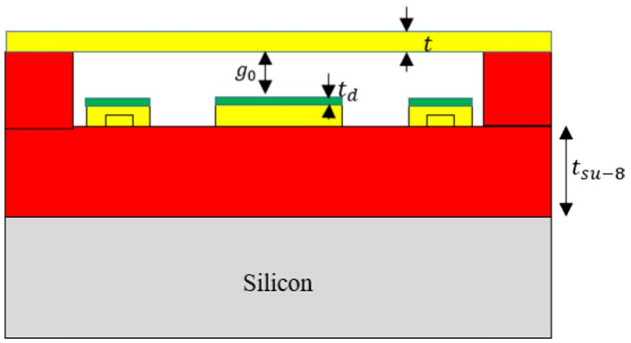

Fig. 2 Side view of the MEMS varactor

spin-coating the substrate with SU-8 layer as shown in Fig. 2, thus greatly increasing its tuning range. The thickness of SU-8 layer ($t_{su\text{-}8}$) was varied from 0 to 30 µm in order to obtain the optimal capacitance ratio and Q-factor. Apart from that, SU-8 is also used as the lateral support for the beams of the varactor. To improve the power handling of the design, a novel horizontal truss aluminium beam with thickness of 2 µm is proposed as shown in Fig. 3.

One of the major failures of RF MEMS varactors is stiction due to dielectric charging effects. One of the effective ways to prevent this issue is to separate RF and DC electrodes for the switch actuation. As such, to increase the reliability of the varactor, a side pull-down configuration and a new stopper design is implemented. The detailed design of the stopper is shown in Fig. 3. A gap of 0.5 µm that exists between the actuator pad and the top beam in the downstate position would prevent direct contact between them. The semi-elliptical at the ground as shown in Fig. 1 further reduces the parasitic capacitance slot. The summary of the proposed design parameters is shown in Table 1.

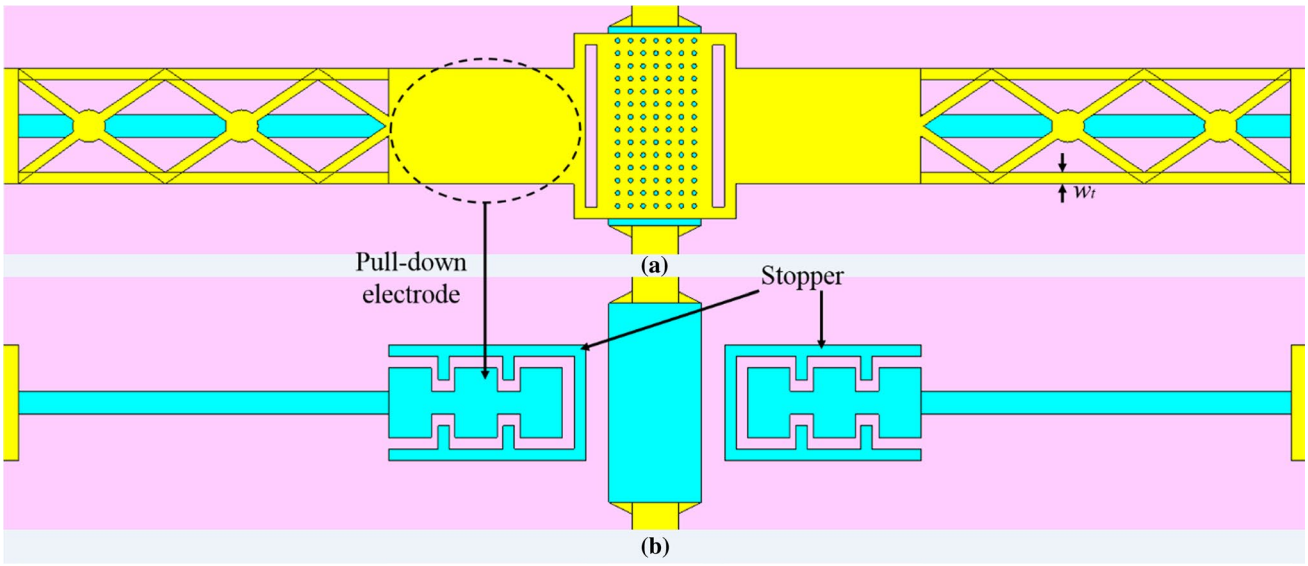

Fig. 3 **a** Top view of side pull-down and stopper with the beam. **b** Side pull-down and stopper underneath the beam

Table 1 Detailed dimensions of the digital varactor

Symbol	Description	Value
L	Length of the beam	550 μm
g_0	Air-gap	3.1 μm
t_d	Thickness of dielectric layer	0.25 μm
ε_{r1}	Relative permittivity of dielectric layer	7.5
t	Thickness of the beam	2 μm
w_t	Width of the truss beam structure	5 μm
t_s	Silicon substrate thickness	525 μm
ρ	Resistivity of silicon substrate	10 k Ω m
W	Width of the co-planar waveguide transmission line	80 μm
G	Gap of the co-planar waveguide transmission line	50 μm
A_1	Area of bit-1 of the varactor	10 μm × 40 μm
A_2	Area of bit-2 of the varactor	20 μm × 40 μm
A_3	Area of bit-3 of the varactor	40 μm × 40 μm
A_4	Area of bit-4 of the varactor	80 μm × 40 μm
A_5	Area of bit-5 of the varactor	160 μm × 40 μm
$t_{SU\text{-}8}$	Thickness of SU-8 layer	0, 5, 10,15, 20, 25, 30 μm
ε_{r2}	Relative permittivity of SU-8	4
tan $\delta_{SU\text{-}8}$	Loss tangent of SU-8	0.04
A_{el}	Area of pull-down electrode	1.82×10^{-9} μm^2
E	Young's modulus of aluminium	69 GPa
V_p	Pull-down voltage	30.31 V
V_h	Holding voltage	25 V
k_T	Spring constant	1.33 N/m
$C_{d(\max)}$	Maximum capacitance value	3.57 pF
$C_{u(\min)}$	Minimum capacitance value	102.23 fF
C_r	Capacitance ratio	35.7

3 Results and discussions

The proposed MEMS varactor design has been simulated in CST Microwave Studio to evaluate and analyse its RF characteristics. Optimisation of SU-8 layer thickness has been done by varying its thickness to achieve two main goals which are high capacitance ratio and improved Q-factor. On the other hand, the mechanical analysis of the beam structure was conducted via CoventorWare™.

3.1 Electro-magnetic simulations

A high resistivity silicon substrate, $\sigma = 0.01$ S/m ($\rho = 10$ k Ω cm) was used to improve the RF performance of the proposed varactor. Based on the Smith chart in Fig. 4, capacitance values and the Q-factor of the varactor can be extracted from the S11 plot using Eqs. (4) and (5) (Rebeiz 2003)

$$C = -\frac{1}{2\pi f X}, \tag{4}$$

$$Q = \frac{Im(Z_{in})}{Re(Z_{in})} \tag{5}$$

The optimal thickness of the SU-8 layer was achieved by comparing the capacitance ratio and the Q-factor for seven different thickness values which are 0, 5, 10, 15, 20, 25 and 30 µm. The simulated results of the respective thickness are tabulated in Table 2. It can be seen that by increasing the thickness of the SU-8, the capacitance ratio of the varactor increases. However, the maximum capacitance ratio is obtained when the thickness is 20 µm while by placing the varactor directly on the silicon substrate results in the lowest capacitance ratio. This is due to less fringing field between the varactor and the SU-8 due to its lower dielectric constant compared to silicon. Q-factor of 812 and 50 were achieved for the $C_{u(\min)}$ and the $C_{d(\max)}$ respectively for the thickness of 20 µm. This shows that good RF performance could also be realised by using thick SU-8 as the passivation layer.

Table 2 Capacitance ratio and Q-factor for different thickness of SU-8

Thickness (µm)	Capacitance ratio	Q-factor (upstate/downstate)
0	16.9	248/95
5	24.5	505/114
10	28.9	613/108
15	34.4	762/93
20	34.8	812/50
25	34.6	648/66
30	33.5	827/62

The power handling capability of the varactor is calculated by simulating the pull-in voltage, V_p between the beam and the centre conductor for the largest bit switch since the RF power is induced on the centre conductor. The maximum RF power before self-actuation is calculated using Eq. (6) (Rebeiz 2003).

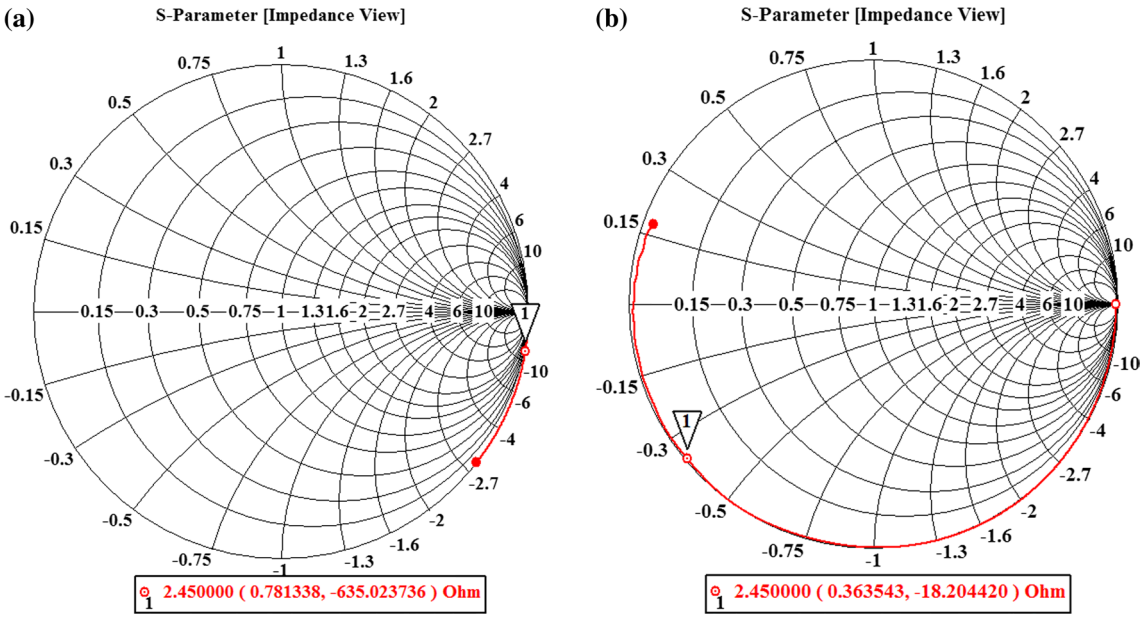

Fig. 4 Simulated S11 of the MEMS varactor from 0 to 10 GHz **a** state 1 (all beams on upstate), **b** state 32 (all beams on downstate)

$$P = \frac{V_p^2}{Z_0} \tag{6}$$

where P is the incident RF power, Z_0 is the characteristic impedance of the line. In addition, the dielectric strength of SU-8 is 4.43 ± 0.16 MV cm^{-1} which is remarkably high for a polymer material. It is reported that for 15 µm thick SU-8 has voltage breakdown of around 7 kV and increases over the thickness (Melai et al. 2009). The simulated pull-in voltage V_p from the centre conductor is 10.5 V and the calculated maximum RF power is 2.2 W. There are 32 capacitance steps which change linearly from 102.23 fF to 3.57 pF with an incremental capacitance step of 0.11 pF as demonstrated in Fig. 5.

3.2 Mechanical simulations

The structure of the truss beam as shown in Fig. 1 was analysed using CoventorWare™ to calculate the pull-in and the holding voltage. In order to obtain similar pull-in voltage for all beams, the beam width is fixed at 50 µm. All the five beams were simulated to calculate their pull-in voltage. The side pull-down pads were implemented to separate the DC voltage and RF voltage to reduce dielectric charging. An incremental positive bias voltage was applied at the pull-down pads while DC potential of the beam is kept at 0 V. The simulated pull-in voltages are within the range of 28–32 V. The discrepancies are mainly due to different sizes of the centre structure of the beams. On the other hand, the lift off or holding voltage analysis was conducted by decreasing the voltage from pull-in voltage until the beam was released to its initial up-state position. Figure 6 shows the pull-in voltage for the 80 µm centre width beam is 30 V while its holding voltage is 25 V. The beam deformation during pull-in voltage is shown in Fig. 7 and the red colour in the centre of the beam determines the maximum displacement. The displacement value of 1.8 µm is more than the one-third of the gap height indicating that mechanical instability had occurred and the beam was pulled down. To investigate the effects of in-plane residual stress and stress

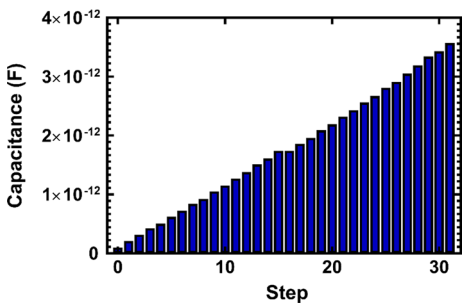

Fig. 5 32 capacitance steps of the variable capacitor

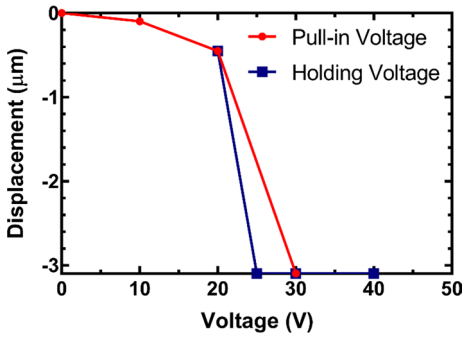

Fig. 6 Pull-in voltage and hold in voltage for 80 µm beam

gradient on the beam, different values of both stresses were simulated. Generally, the biaxial residual stress introduced on the MEMS structure is due to fabrication process. In this work, in-plane residual stress of 0, 50 and 100 MPa were chosen to analyse its effect on the spring constant of the proposed beam (Reines et al. 2009; Yang et al. 2014). As comparison, a solid fixed–fixed beam of similar configuration (length = 550 µm, width = 50 µm and t = 2 µm) was also analysed. The sensitivity analysis due the residual stress for both beams was carried out. In addition, vertical stress gradients of 0 to ±8 MPa/µm were induced on the beam structure to analyse its initial displacement. Further analysis will be discussed in Sects. 3.3.1 and 3.3.2.

3.3 Modal analysis

Modal analysis of the beam varactor was carried out to compute the mechanical natural frequencies of the structure at equilibrium. The calculated frequencies and their associated mode shapes are shown in Fig. 8. The finding of these frequencies helps to understand how the beam

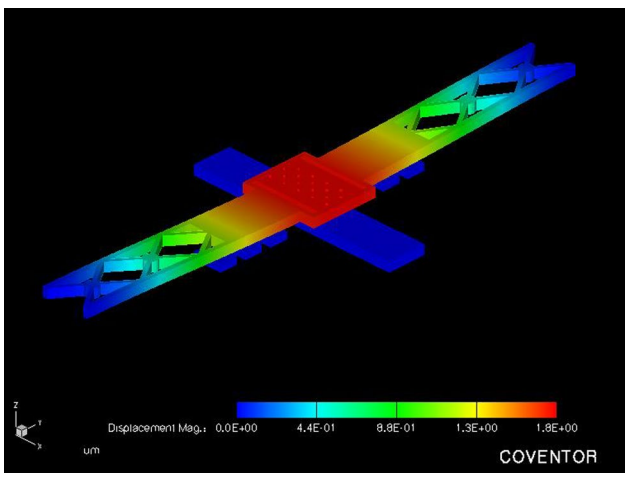

Fig. 7 Beam displacement when the pull-in voltage applied

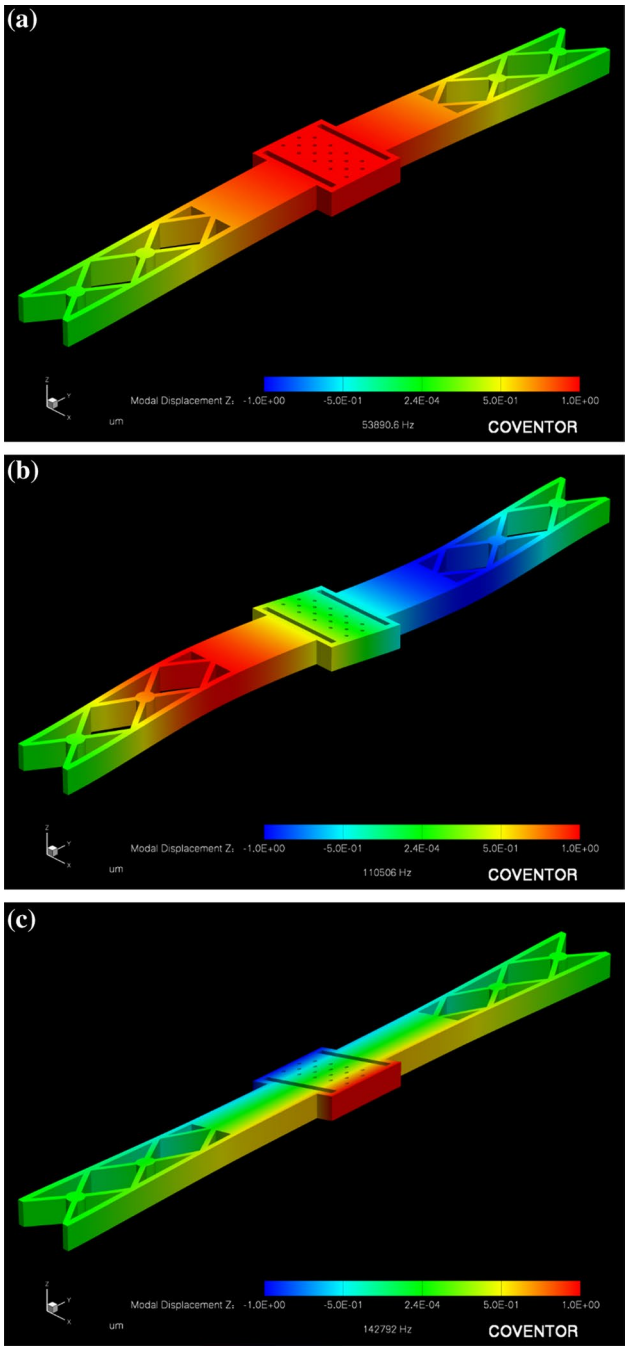

Fig. 8 Mechanical resonant frequencies of the beam at **a** 53.9 kHz, **b** 110.5 kHz and **c** 142.8 kHz

would respond to the surrounding noise. The resonance frequencies of the 80 μm beam is at 53.9, 110.5 and 142.8 kHz. These resonances occur without any external force applied to the beam structure. In addition, the switching speed of the beam can be estimated by one-quarter period of the mechanical primary natural frequency of the beam (Goldsmith et al. 1999). This results the theoretical switching speed of 4.64 μs.

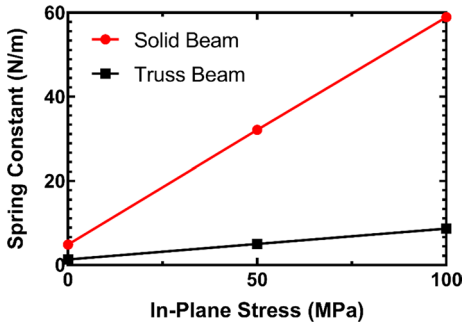

Fig. 9 Simulated spring constant versus in-plane stress

3.3.1 *In-plane stress*

The total spring constant, k_T of a mechanical beam is given by the summation of spring constant due to mechanical properties of the beam, k_1 and stress-induced spring constant after fabrication process, k_2. The total spring constant is then calculated as

$$k_T = k_1 + k_2 \tag{7}$$

The spring constant of the beam is calculated by finding its pull-in voltage and using equation (Rebeiz 2003)

$$V_p = \sqrt{\frac{8k_T g_0^3}{27\varepsilon_0 A_e}} \tag{8}$$

The total spring constant of the beam without residual stress is 1.33 N/m while for the solid beam design is 4.88 N/m. The corresponding pull-in voltages are 30.31 and 58.2 V respectively. This shows that the proposed beam can reduce the actuation voltage by almost 50%. The advantage of the truss beam over conventional solid beam design could be further emphasised by comparing its sensitivity to in-plane residual stress. Both designs were simulated with in-plane residual stress of 0, 50 and 100 MPa. The simulated spring constants against residual stress are shown in Fig. 9. It can be seen that the spring constant of the truss beam increases by only 3 N/m for a residual stress of 50 MPa which results in a maximum k_2/k_1 ratio of 2.6 as shown in Fig. 10. As comparison, the solid beam structure will result in a k_2/k_1 ratio of 5 demonstrating its higher sensitivity to in-plane residual stress.

3.3.2 *Stress gradients*

The beam structure was also simulated versus varying vertical stress gradients. The deformation of the centre plate along the beam length direction due to vertical stress gradient of 0 to ±8 MPa/μm are shown in Fig. 11. The simulation results show that positive stress gradients cause the beam to deflect downward while negative stress deflect the beam in

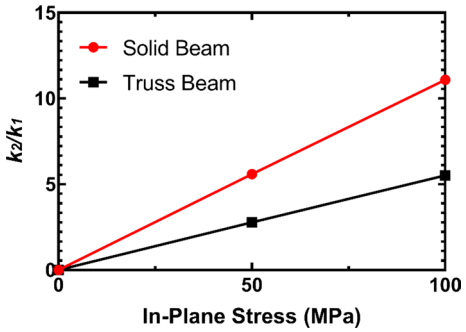

Fig. 10 k_2/k_1 ratio versus in-plane stress

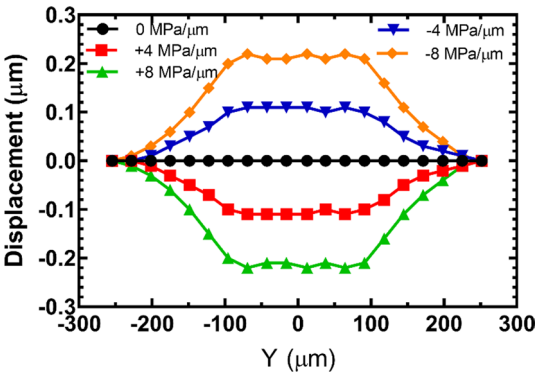

Fig. 11 Simulated displacement in the centre plate of the truss beam versus vertical stress gradient

the opposite direction. A stress gradient of ±8 MPa/μm will result in maximum centre displacement of 0.3 μm which is still within the acceptable range (Reines et al. 2009).

3.3.3 Von Mises stress

Further simulation on the von Mises stress was undertaken in order to investigate the stress on the beam during actuation. This analysis is important to ensure the beam structure can withstand the maximum applied force. Figure 12 shows that the maximum von Mises stress is located at the end of the beam. These values are lower than the yield strength of aluminium (124 MPa) and gives a clear indication that the beam would not break when actuated.

4 Proposed fabrication process

Below are the overview of the proposed fabrication process for the varactor design. The fabrication process of the MEMS varactor composes of several steps described using the following diagram in Fig. 13. A 525 μm thick high resistivity silicon wafer is chosen as the substrate.

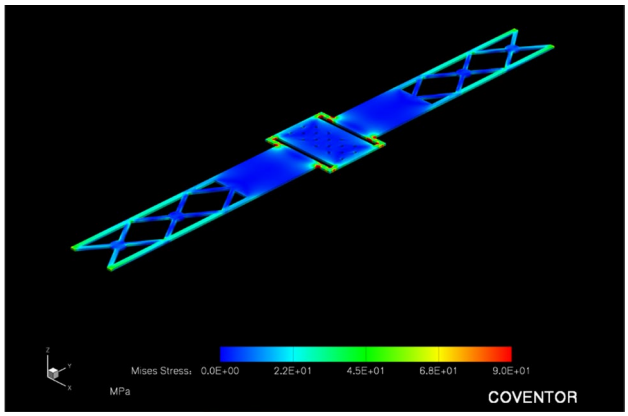

Fig. 12 Von Misses stress for truss beam

A total of five masks are required for the fabrication process. First, 20 μm of SU-8 is spin-coated on the surface of silicon wafer. Then, the SU-8 is soft baked to evaporate the solvent before it can be exposed under the UV light. Next, post exposure bake (PEB) is performed. To further cross-link and cure the SU-8 layer, hard bake is needed at temperature 210 °C for 1 h. As a precaution, the SU-8 cannot be baked at a very high temperature (exceeding 300 °C) to avoid crack in the film and it must be more than subsequence process temperature to make it withstands the temperature. As for this process, the subsequence process must not exceed 200 °C. After curing the SU-8, 2 μm of thickness of Al is sputtered and patterned using dry etching process to form the CPW transmission lines and stopper. In the next step, 1.5 μm Al is deposited and patterned using lift-off process to define the side pull-down electrode. Then, thin tantalum nitride (TaN) is patterned by lift-off process to form the bias lines after deposition. By using plasma enhanced chemical vapour deposition (PECVD) technique, 2500 Å Si3N4 is patterned on top of the centre conductor, stopper, and pull-down electrode as dielectric layer. In this process, 150 °C instead of 300 °C for plated shower is used to make sure it will not affect the SU-8 layer. Next, around 7 μm thickness of polymer or any sacrificial layer such as SU-8 or polyimide is spin coated and cured up to 200 °C to form the anchor and sacrificial layer (Lucibello et al. 2013). Adhesion between the sacrificial layer material and SU-8 is needed to be taken to account. Common sacrificial layer such as silicon oxide is not suitable for this work due to poor adhesion to the SU-8. Then, chemical mechanical polishing (CMP) technique is then used to level the SU-8 to get around 5.35 μm for the anchor and sacrificial layer. Then, 2 μm Al is deposited and patterned to form the beam and ground. The sacrificial layer then will be removed using oxygen plasma to release the beam.

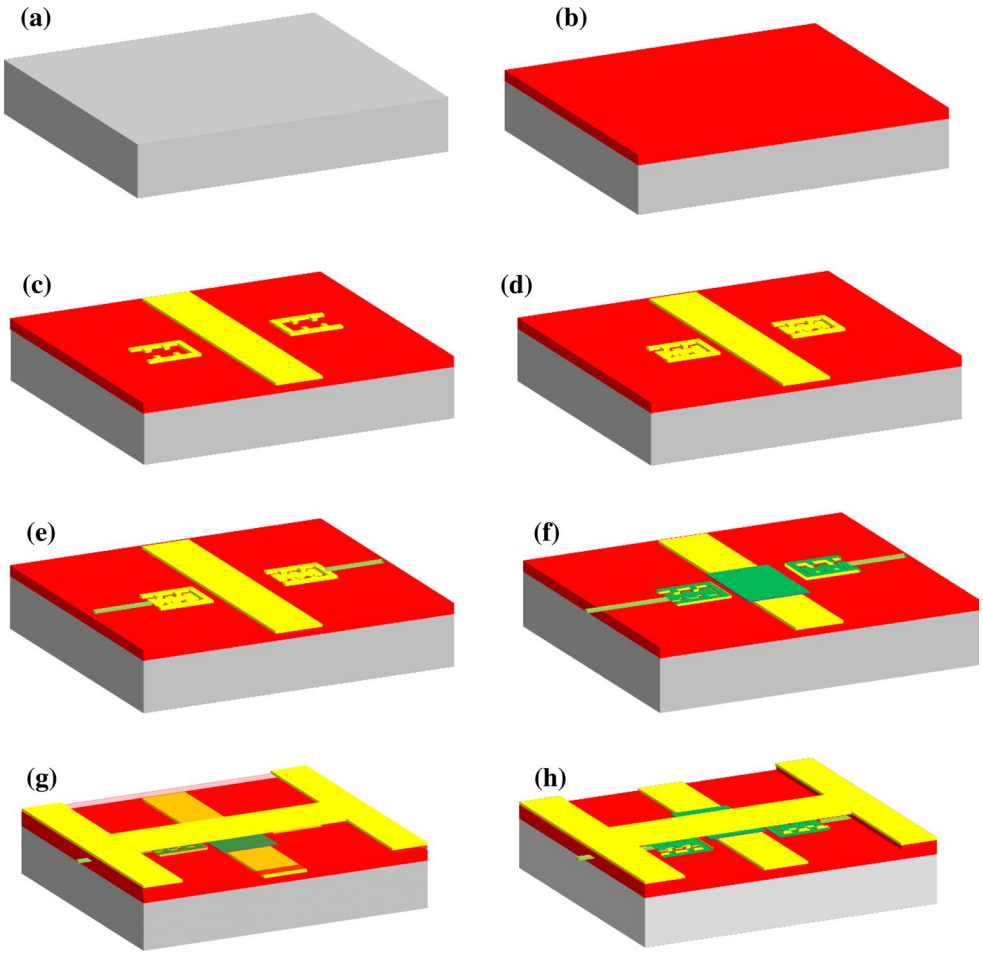

Fig. 13 Proposed fabrication process of the devices. **a** High resistivity silicon. **b** Spin coat of SU-8. **c** Deposit and pattern of Al for CPW and stopper. **d** Deposit and pattern of Al for pull-down electrode. **e** Deposit and pattern TaN for bias line. **f** Deposit and pattern Si_3N_4 for dielectric layer. **g** Deposit sacrificial layer and CMP. **h** Remove sacrificial layer. *Gray rectangle* Si, *red rectangle* SU-8, *yellow rectangle* Al, *light green rectangle* TaN, *dark green rectangle* Si_3N_4, *pink rectangle* sacrificial layer

5 Conclusion

This paper has presented the design, simulation and analysis of a 5-bit RF MEMS varactor for wireless applications. In this paper, thick SU-8 polymer has been implemented as a base structure to elevate the varactor from the silicon substrate to achieve high capacitance ratio. The thickness of the SU-8 layer has been optimized using simulation tool in order to get the optimum capacitance ratio and Q-factor which is 35 and 812 respectively. Besides that, the advantages of the truss beam structure over conventional doubly clamped solid beam design has been analysed and highlighted in terms of spring constant, pull-in voltages, in-plane stress and gradient stress effects. The proposed truss beam has shown it can reduce almost 50% of actuation voltage from solid beam and has less sensitivity to in-plane stress during the fabrication. The proposed varactor design could be applied to reconfigurable and multi-band RF front end components such as tunable filters, impedance matching networks and phase shifters.

References

Bakri-kassem M (2007) Novel RF MEMS varactors realized in standard MEMS and CMOS processes

Dussopt L, Rebeiz GM (2003) An X- to Ku-band 3-bit digital MEMS varactor. IEEE Microw Wirel Compon Lett 13(9):361–363. doi:10.1109/LMWC.2003.817118

Goldsmith CL, Malczewski A, Yao ZJ, Chen S, Ehmke J, Hinzel DH (1999) RF MEMs variable capacitors for tunable filters. Int J RF Microw Comput Aided Eng 9(4):362–374. doi:10.1002/(SICI)1099-047X(199907)9:4<362:AID-MMCE7>3.0.CO;2-H

Gupta P, Singh P, Srivastava P (2013) Design and analysis of RF MEMS varactor for extended tuning range. In: 2013 international conference on control, computing, communication and materials (ICCCCM). IEEE, New York, pp 4–7. doi:10.1109/ICCCCM.2013.6648915

Lucibello A, Proietti E, Giacomozzi F, Marcelli R, Bartolucci G, De Angelis G (2013) RF MEMS switches fabrication by using SU-8 technology. Microsyst Technol 19(6):929–936. doi:10.1007/s00542-013-1753-8

Marcelli R, Catoni S, Frenguelli L (2008) Low-loss microwave interconnections by using polymeric based coplanar waveguides on low resistivity silicon substrates. Microelectron Eng 85(2):425–431. doi:10.1016/j.mee.2007.08.002

McFeetors G, Okoniewski M (2007) Performance and operation of stressed dual-gap RF MEMS varactors. In: Proceedings of the 36th European microwave conference, EuMC 2006, 10(September). IEEE, New York, pp 1064–1067. doi:10.1109/EUMC.2006.281117

Melai J, Salm C, Smits S, Blanco Carballo VM, Schmitz J, Hageluken B (2007) Considerations on using SU-8 as a construction material for high aspect ratio structures. In: 10th annual workshop on semiconductor advances for future electronics and sensors (SAFE). pp 29–534

Melai J, Salm C, Smits S, Visschers J, Schmitz J (2009) The electrical conduction and dielectric strength of SU-8. J Micromech Microeng 19(6):65012. doi:10.1088/0960-1317/19/6/065012

Patel CD, Rebeiz GM (2012) High-Q 3 b/4 b RF MEMS digitally tunable capacitors for 0.8–3 GHz applications. IEEE Microw Wirel Compon Lett 22(8):394–396. doi:10.1109/LMWC.2012.2205301

Ramli NA, Arslan T, Haridas N, Zhou W (2016a) Design and modelling of a digital MEMS varactor for wireless applications. In: 7th international conference on thermal, mechanical and multi-physics simulation and experiments in microelectronics and microsystems (EuroSimE). IEEE, New York, pp 3–7. doi:10.1109/EuroSimE.2016.7463383

Ramli NA, Arslan T, Haridas N, Zhou W (2016b) Design and simulation of a high tuning range MEMS digital varactor using SU-8. In: symposium on design, test, integration and packaging of MEMS/MOEMS, DTIP 2016. pp 1–6. doi:10.1109/DTIP.2016.7514842

Rebeiz GM (2003) RF mems-theory, design and technology, vol 53. Wiley, New York. doi:10.1017/CBO9781107415324.004

Reines I, Pillans B, Rebeiz GM (2009) A stress-tolerant temperature-stable RF MEMS switched capacitor. In: Proceedings of the IEEE international conference on micro electro mechanical systems (MEMS). IEEE, New York, pp 880–883. doi:10.1109/MEMSYS.2009.4805524

Reinke JR (2011) CMOS-MEMS variable capacitors for reconfigurable RF circuits

Yang HH, Zareie H, Rebeiz GM (2014) A high power stress-gradient resilient RF MEMS capacitive switch. J Microelectromech Syst 24(3):599–607. doi:10.1109/JMEMS.2014.2335173